Journal of Alloys and Compounds 509 (2011) 10055–10061

Contents lists available at ScienceDirect

Journal of Alloys and Compounds

journal homepage: www.elsevier.com/locate/jallcom

New process for synthesis of ZnO thin films: Microstructural, optical and electrical characterization

S.L. Patil[a], M.A. Chougule[a], S.G. Pawar[a], B.T. Raut[a], Shashwati Sen[b], V.B. Patil[a,*]

[a] Materials Research Laboratory, School of Physical Sciences, Solapur University, Solapur 413255, M.S., India
[b] Crystal Technology Section, Technical Physics Division, BARC, Mumbai, M.S., India

ARTICLE INFO

Article history:
Received 1 July 2011
Received in revised form 2 August 2011
Accepted 6 August 2011
Available online 12 August 2011

Keywords:
Sol gel method
XRD
EDAX
HRTEM
SEM
Band gap

ABSTRACT

Nanocrystalline ZnO thin films were prepared on glass substrates by using spin coating technique. The effect of annealing temperature (400–700 °C) on structural, compositional, microstructural, morphological, electrical and optical properties of ZnO thin films were studied by X-ray diffraction (XRD), Energy dispersive Spectroscopy (EDS), Atomic Force Microscopy (AFM), High Resolution Transmission Microscopy (HRTEM), Scanning Electron Microscopy (SEM), Electrical conductivity and UV–visible Spectroscopy (UV–vis). XRD measurements show that all the films are nanocrystallized in the hexagonal wurtzite structure and present a random orientation. The crystallite size increases with increasing annealing temperature. These modifications influence the optical properties. The AFM analysis revealed that the surface morphology is smooth. The HRTEM analysis of ZnO thin film annealed at 700 °C confirms nanocrystalline nature of film. The SEM results shows that a uniform surface morphology and the nanoparticles are fine with an average grain size of about 40–60 nm. The dc room temperature electrical conductivity of ZnO thin films were increased from 10^{-6} to 10^{-5} $(\Omega\,cm)^{-1}$ with increase in annealing temperature. The electron carrier concentration (n) and mobility (μ) of ZnO films annealed at 400–700 °C were estimated to be of the order of $4.75–7.10 \times 10^{19}$ cm^{-3} and $2.98–5.20 \times 10^{-5}$ $cm^2\,V^{-1}\,S^{-1}$.

The optical band gap has been determined from the absorption coefficient. We found that the optical band gap energy decreases from 3.32 eV to 3.18 eV with increasing annealing temperature between 400 and 700 °C. This means that the optical quality of ZnO films is improved by annealing.

It is observed that the ZnO thin film annealing at 700 °C has a smooth and flat texture suited for different optoelectronic applications.

1. Introduction

Zinc oxide (ZnO) is an interesting wide-band-gap semiconductor material with a direct band gap of 3.36 eV [1] at room temperature and exciton binding energy of 60 meV. It has crystalline structure of the wurtzite type and the unit cell with the constants $a = 3.24$ Å and $c = 5.19$ Å. Thin films of ZnO are utilized for a wide variety of electronic and opto-electronic applications, such as surface acoustic wave devices [4], transparent conducting electrodes [2], heat mirrors [3]. Nanoscale porous structures of ZnO with a high surface area find their application in chemical sensors [5] and dye-sensitised solar cells [6]. Various techniques have been used to deposit undoped and doped ZnO films on different substrates, including spray pyrolysis [7], organometallic chemical vapor deposition [8], pulsed laser deposition [9], sputtering [10], and sol–gel process [11]. Among these, the sol–gel technique is credited with several advantages, such as deposition of high purity, homogeneous, cheaper, large-area films at relatively low temperatures. There are scarcely any reports on the effect of annealing temperature on structure, morphology, microstructure, electrical transport and optical properties of ZnO films prepared by the sol–gel spin coating technique.

In this paper, we concentrate on the structural, compositional, microstructural, morphological, electrical transport and optical properties of sol–gel derived ZnO films deposited by spin coating technique.

Estimates of various structural and optoelectronic parameters such as grain size, composition, roughness, dc conductivity, thermoelectric power, carrier concentration, mobility, absorption coefficient and band gap have been made.

2. Experimental details

Nanosized ZnO thin films have been synthesized by a sol–gel spin coating technique using Zinc acetate dihydrate ($Zn(CH_3CO_2)_2{\cdot}2H_2O$) as a source of zinc oxide. In

* Corresponding author. Tel.: +91 2172744770; fax: +91 2172744770.
E-mail address: drvbpatil@gmail.com (V.B. Patil).

0925-8388/$ – see front matter © 2011 Elsevier B.V. All rights reserved.
doi:10.1016/j.jallcom.2011.08.030

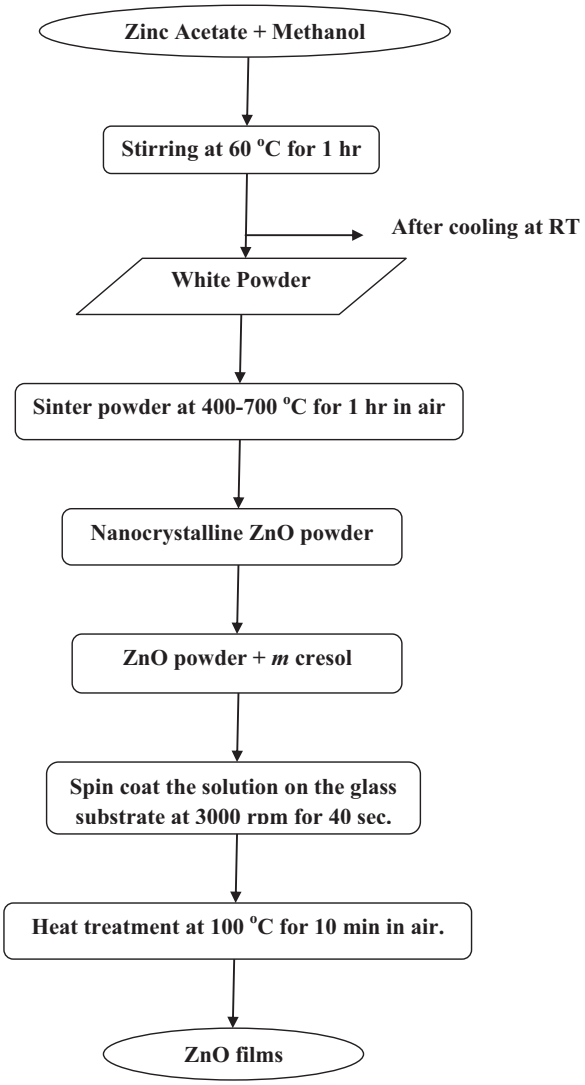

Fig. 1. Flow diagram for ZnO films prepared from the sol–gel spin-coating technique.

a typical experiment; Zinc acetate dihydrate was added to 40 ml of methanol and stirred vigorously at 60 °C for 1 h, leading to the formation of white color powder. The as prepared powder was sintered at various temperatures ranging from 400 to 700 °C with a fixed annealing time of 1 h in an ambient air to obtain nanocrystalline ZnO powder with different crystallite sizes. The nanocrystalline ZnO powder was further dissolved in *m*-cresol and solution was continuously stirred for 11 h at room temperature and filtered. The filtered solution was deposited on to a glass substrate by a single wafer spin processor (APEX Instruments, Kolkata, Model SCU 2007). After setting the substrate on the substrate holder of the spin coater, the coating solution (approximately 0.2 ml) was dropped and spin-casted at 3000 rpm for 40 s in an air and dried on a hot plate at 100 °C for 10 min. Fig. 1 shows the flow diagram for the sol gel synthesis and deposition of ZnO films by spin-coating technique. X-ray powder diffraction (XRD) pattern of the prepared films were measured for the phase identification and estimation of the average crystallite size. XRD measurements were made by a Philips PW-3710 model system. The (1 0 1) diffraction peak has been considered for crystallite size estimation. High resolution transmission electron microscopy (HRTEM) and small area electron diffraction (SAED) were obtained in order to investigate the morphology and structure of zinc oxide thin films. The HRTEM images were taken with a Hitachi Model H-800 transmission electron microscope. Energy-dispersive X-ray analyses were recorded on a JEOL-2010 TEM. Roughness of the film was determined from the Atomic force microscopy (AFM) using AFM, SPA 300 HV. In order to determine the particle size and morphology of nanopowder, the sintered powders were dispersed in *m*-cresol and sonicated ultrasonically by using OSCAR ultra sonic bath apparatus, to separate out individual particles. The size and morphology of the thin films were then observed on SEM Model: JEOL JSM 6360 operating at 20 kV. The dc electrical conductivity measurements of ZnO thin films were performed using four probe technique in 300–500 K temperature range. The optical absorption spectra of the ZnO thin films were measured using a double-beam spectrophotometer Shimadzu UV-140 over 200–1000 nm wavelength range.

3. Results and discussions

3.1. Growth mechanism and film formation of ZnO

The growth mechanism of ZnO film formation by the sol gel spin coating method can be enlightened as follows:

$$Zn(CH_3COO)_2{\cdot}2H_2O + 2CH_3\text{-}OH \rightarrow Zn(OH)_2 + 2CH_3COOCH_3 + 2H_2O$$

Since to improve crystallinity and remove hydroxide phase, powders were annealed between 400 and 700 °C for 1 h pure ZnO is formed after air annealing by following mechanism:

$$Zn(OH)_2 \downarrow + \text{Carbonaceous compounds} \xrightarrow[\text{Oxidation}]{\text{Air annealing}} ZnO + H_2O \uparrow$$

Thin films of annealed ZnO nanopowders are formed using organic solvent m-cresol as discussed in Section 2.

The deposited films were found to be strongly adhering to the glass substrate and they appeared in light yellow color. The thickness of ZnO films on the glass substrate were calculated using gravimetric weight difference method using formula:

$$t = \frac{m}{A\rho} \quad (1)$$

where t is film thickness of the film; m is actual mass deposited onto substrate; A is area of the film and ρ is the density of zinc oxide (5.606 g/cm^3).

It was observed that increasing the annealing temperature (400–700 °C) resulted in a decrease in film thickness. The ZnO film thickness is also confirmed by Dektak profilometer and is nearly equal to weight difference method and is presented in Table 1.

3.2. Structural analysis

Fig. 2 shows X-ray diffraction patterns of ZnO thin films deposited on glass substrates by spin-coating technique at different annealing temperatures of 400, 500, 600, and 700 °C. The X-ray spectra show well-defined diffraction peaks showing good crystallinity. The crystallites are randomly oriented and the *d*-values calculated for the diffraction peaks are in good agreement with those given in JCPD data card (79.0208) for ZnO. This means that

Table 1
Interplanar spacing's deduced from electron diffraction patterns reported in Fig. 5(b) together with the corresponding ones obtained from literature data. Numbers in brackets (n) represent the labels of reflections in diffraction patterns.

Interplanar spacings determined in this work on ZnO films		Interplanar spacing's reported in literature[a]	
(n)	d (nm)	d (nm)	hkl
(1)	0.2825	0.2821	1 0 0
(2)	0.2622	0.2610	0 0 2
(3)	0.2481	0.2486	1 0 1
(4)	0.1918	0.1918	1 0 2
(5)	0.1623	0.1632	1 1 0

[a] Joint Commission Powder Diffraction File No. (79.0208).

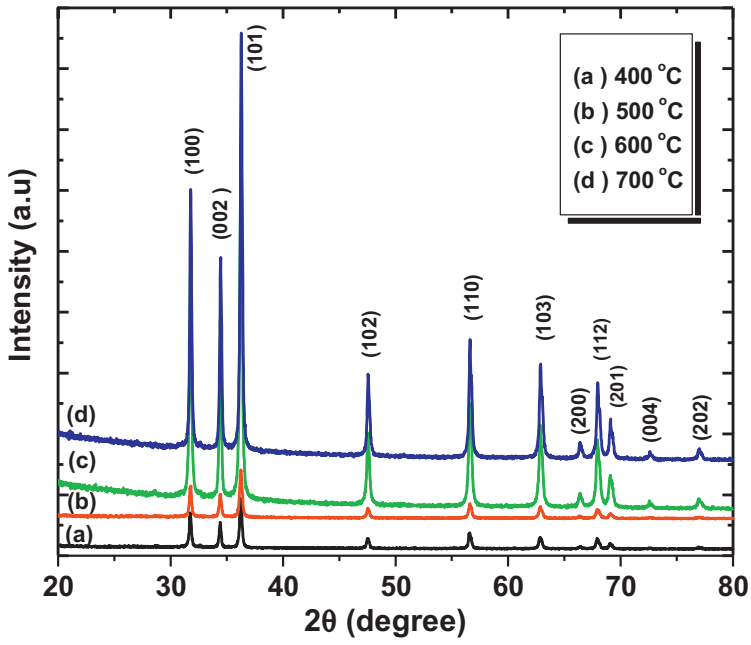

Fig. 2. X ray diffraction patterns of ZnO films annealed at different temperatures (400–700 °C).

ZnO has been crystallized in a hexagonal wurtzite form. The lattice constants calculated from the present data for (1 0 1) phase (strong reflection) are $a = 3.265$ Å and $c = 5.214$ Å, respectively.

From Fig. 2, eight prominent peaks, corresponding to the (1 0 0) phase ($2\theta \approx 31.65°$), (0 0 2) phase ($2\theta \approx 64.47°$), (1 0 1) phase ($2\theta \approx 36.18°$), (1 0 2) phase ($2\theta \approx 47.52°$), (1 1 0) phase ($2\theta \approx 56.49°$), (1 0 3) phase ($2\theta \approx 62.79°$), (1 1 2) phase ($2\theta \approx 67.97°$) and (2 0 1) phase ($2\theta \approx 69.24°$) XRD peaks were observed, and it is concluded that all the films were polycrystalline with a hexagonal wurtzite structure [JCPD: 79.0208, a = 3.2628 Å and $c = 5.2194$ Å] and a random orientation, which generally occurs in the growth of ZnO thin films [12–14].

The average particle sizes of ZnO thin films were calculated using the full width at half maximum (FWHM) of (1 0 1) peak from the Scherrer's method (Eq. (2)) and are presented in Table 2.

$$D = \frac{C\lambda}{\beta \cos\theta} \tag{2}$$

where β is the full width at half maximum of X-ray peak in radians, D is the crystallite size, λ is the X-ray wavelength and C is the correction factor taken as 0.90 in the calculation.

The calculated value of the crystallite sizes varies between 61.82 and 73.48 nm when ZnO film annealed between 400 and 700 °C. It was observed that crystallite size increased with increasing annealing temperature, which can be understood by considering the merging process induced from thermal annealing. For ZnO nanoparticles, there are many dangling bonds related to the Zinc and oxygen defects at the grain boundaries. As a result, these defects are favorable to the merging process to form larger ZnO grains while increasing the annealing temperature. The FWHM of (1 0 1) plane of ZnO thin film with various annealing temperatures is also compared. As the annealing temperature increases from 400 to 700 °C, the FWHM value of ZnO thin film exhibits a tendency to decrease, which can be attributed to the coalescences of grains at higher annealing temperature [12–14]. As a result, it implies that the crystallinity of the ZnO thin films is improved at higher annealing temperatures. Other workers [12,13] have also observed the improvement in crystallinity of the ZnO thin films with the increase of annealing temperature. These may be due to high annealing temperature providing energy to crystallites gaining enough energy to orient in proper equilibrium sites, resulting in the improvement of crystallinity and degree of orientation of the ZnO films.

3.3. Compositional and micro structural analysis

The energy-dispersive X-ray (EDX) spectrometry shown in Fig. 3 clearly shows Zn and O elements in the products with an approximate molar ratio of 1:1 (the Cu signal is attributed to the copper meshes for TEM). AFM (non contact mode) was used to record the topography of the ZnO thin film annealed at 700 °C. In this mode, the tip of the cantilever does not contact with the sample surface. The cantilever is instead oscillated at a frequency slightly above its resonance frequency where the amplitude of oscillation is typically a few nanometers (<10 nm). The surface morphologies of the ZnO nanoparticles exhibit notable features. The surface roughness of the film over a 3 μm × 3 μm area was measured by AFM (Fig. 4(a) and (b). The surface roughness mean square (RMS) of the film is 25 nm, which demonstrates that the surface morphology of ZnO film annealed at 700 °C is smooth. Fig. 5(a) shows HRTEM image of ZnO thin film annealed at 700 °C. It clearly

Table 2
Effect of annealing on ZnO thin film properties.

Sr. no.	Annealing temperature (°C)	Crystallite size, (nm) (from XRD)	Thickness (μm)	Energy gap, E_g (eV)	Activation energy, $E_{a\sigma}$, (eV) HT LT	Carrier (n) concentration, (cm^{-3})	Mobility(μ) ($cm^2\ V^{-1}\ S^{-1}$)
1.	400	61.82	0.37	3.32	0.21 0.010	4.75×10^{19}	2.98×10^{-5}
2.	500	62.29	0.33	3.28	0. 28 0.014	5.20×10^{19}	3.53×10^{-5}
3.	600	64.89	0.32	3.22	0. 40 0.026	6.42×10^{19}	4.50×10^{-5}
4.	700	73.48	0.29	3.18	0.45 0.077	7.10×10^{19}	5.2×10^{-5}

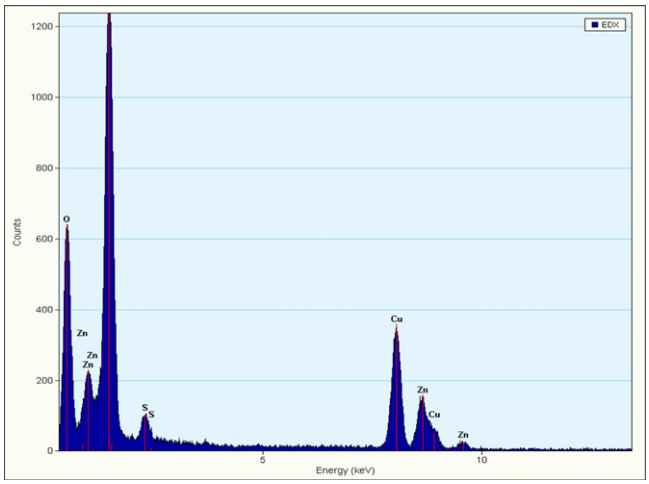

Fig. 3. EDAX spectra of ZnO thin film annealed at 700 °C.

shows that a grain of about 40–60 nm in size is really aggregate of many small crystallites of around 10–20 nm. Fig. 5(b) shows Electron diffraction pattern of ZnO thin film annealed at 700 °C. The different arrangement of dominant diffracted rings indicates a phase evolution of crystalline grains as a consequence of thermal annealing. Table 1 shows the interplanar spacing's determined from diffraction pattern together with the corresponding ones of ZnO wurtzite phases reported in the literature for comparison [12–14].

3.4. Surface morphological studies

The two-dimensional high magnification surface morphologies of ZnO thin films annealed at 400–700 °C were carried out using SEM images are shown in Fig. 6(a)–(d). From the micrographs, it is seen that the film consists of nanocrystalline grains with uniform coverage of the substrate surface with randomly oriented morphology and the crystallite size is increased from 40 to 52 nm as annealing temperature increases from 400 to 700 °C. The crystallite size calculated from SEM analysis is quite in good agreement with that of crystallite size calculated from XRD analysis.

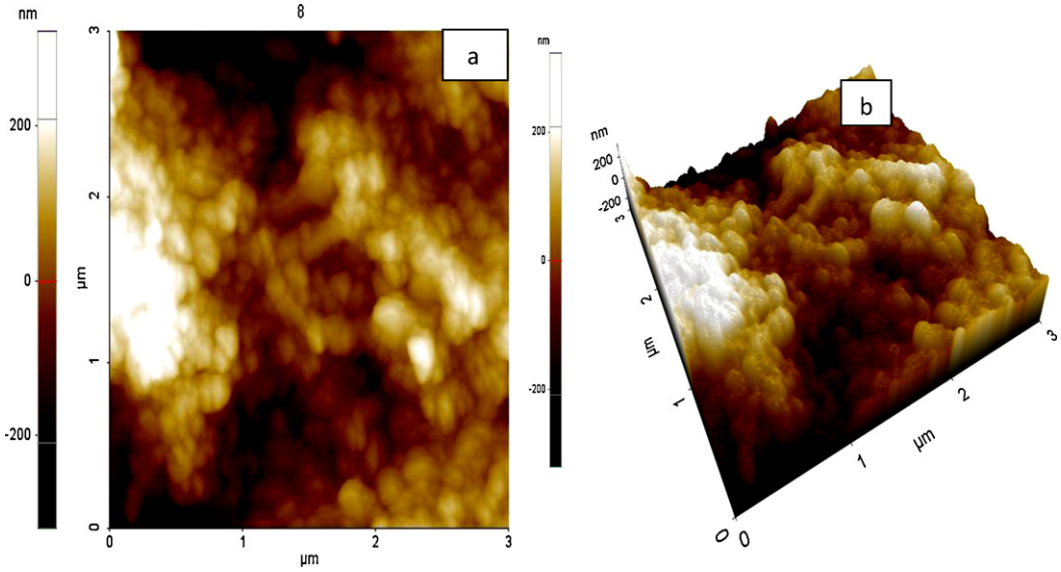

Fig. 4. AFM images of ZnO thin films annealed at 700 °C: (a) Planer view (b) 3D view.

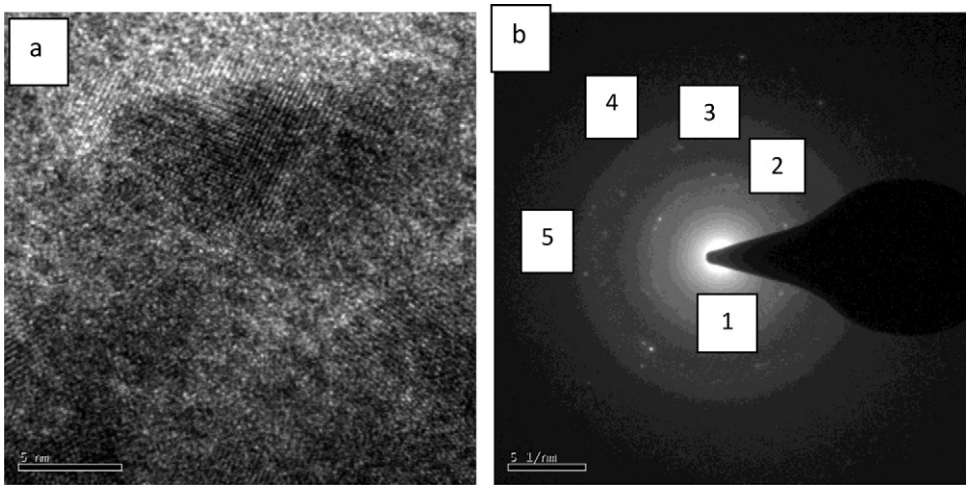

Fig. 5. HRTEM of ZnO thin film annealed at 700 °C: (a) microstructure (b) selected area electron diffraction pattern.

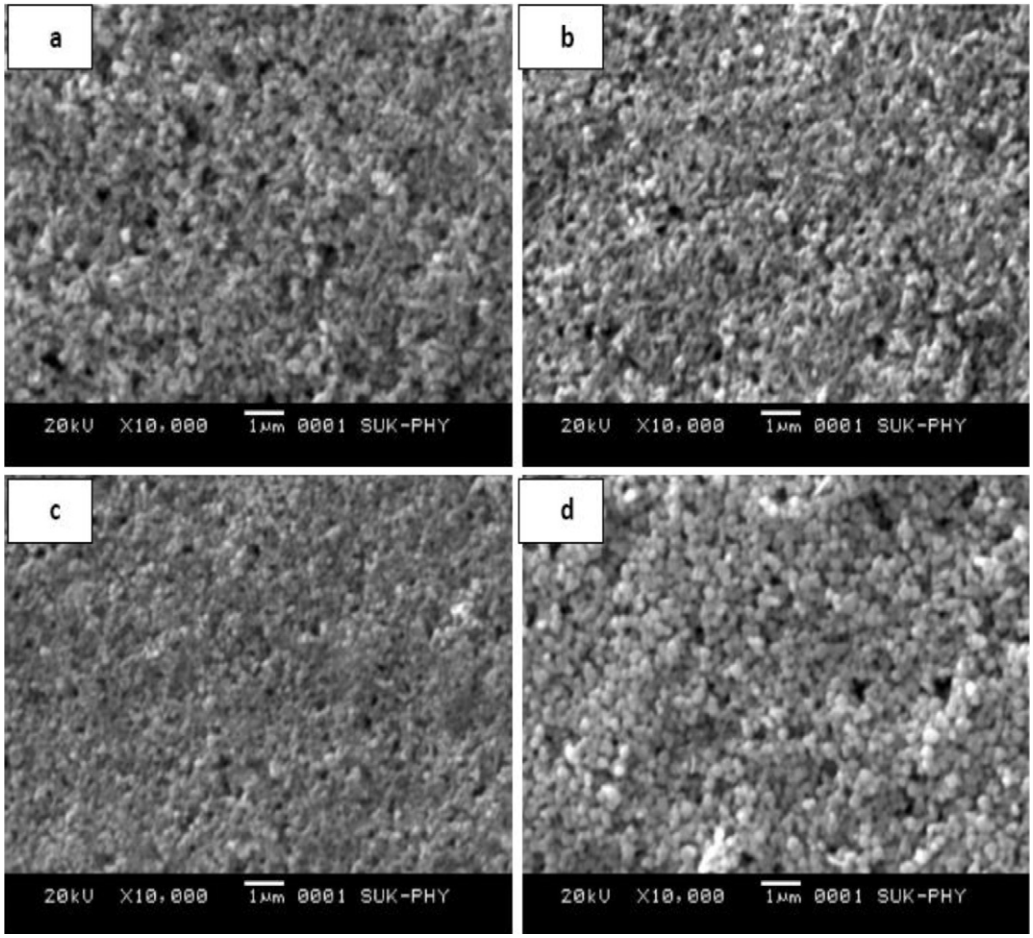

Fig. 6. SEM images of ZnO thin films anneled at (a) 400 °C (b) 500 °C (c) 600 °C and (d) 700 °C.

3.5. Electrical transport studies

3.5.1. DC conductivity measurement

The four-probe technique was employed for measurement of variation of dc electrical conductivity of ZnO film with annealing temperature. The variation of dc conductivity (σ) with reciprocal temperature (1000/T) is depicted in Fig. 7. After annealing, room temperature electrical conductivity was increased from 10^{-6} to $10^{-5}\,(\Omega\,\mathrm{cm})^{-1}$, due to increase in the crystallite size and reduced scattering at the grain boundary. Other workers [12–14] have also observed the increase in conductivity of the ZnO thin films with the increase of annealing temperature.

From Fig. 7 it is observed that the conductivity of film is increases with increase in annealing temperature, further it is observed that conductivity obeys Arrhenius behavior indicating a semiconducting transport behavior. The activation energies were calculated using the relation:

$$\sigma = \sigma_O \exp\left(\frac{-E_a}{kT}\right) \tag{3}$$

where, σ is the conductivity at temperature T, σ_o is a constant, k is the Boltzmann constant, T is the absolute temperature and E_a is the activation energy. The activation energy represents the location of trap levels below the conduction band. From Fig. 7, it is seen that the activation energy (HT) is increases from 0.21 to 0.45 eV, when film annealed between 400 and 700 °C indicating no significant change.

3.5.2. Thermoelectric power measurement

The thermo-emf of ZnO films annealed between 400 and 700 °C was measured as a function of temperature in the temperature range 300–500 K. The polarity of the thermally generated voltage at the hot end was positive, indicating that the ZnO films are of n-type [15,16]. The variation of the thermo-emf (ΔV) with

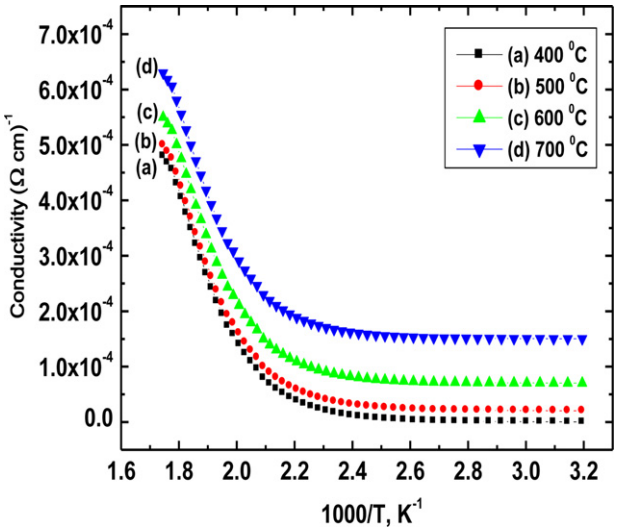

Fig. 7. Plot of dc conductivity versus 1000/T of ZnO thin film annealed at different temperatures (400–700 °C).

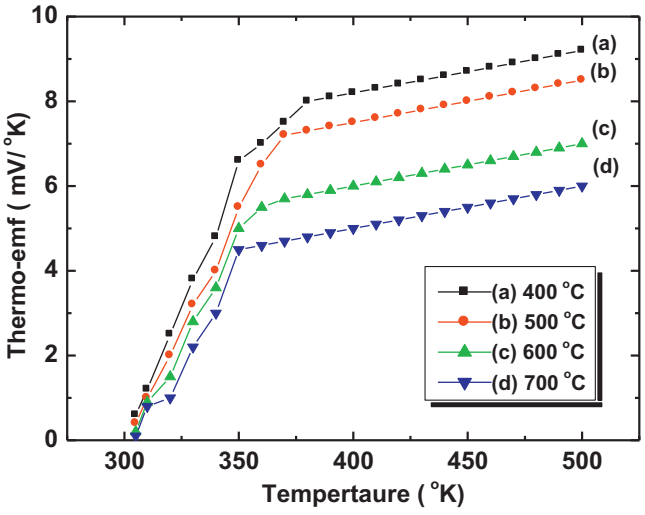

Fig. 8. The variation of thermo-emf with temperature of ZnO thin film annealed at different temperatures (400–700 °C).

temperature is shown in Fig. 8. The thermo-emf increases with increasing temperature. The thermo-electric power (TEP) was used to evaluate the carrier mobility (μ) and carrier concentration (n) using the relation,

$$\mathrm{TEP} = -\frac{k}{e}[A + \ln\{2(2\pi m_c{}^* kT)^{3/2}/nh^3\}] \quad (4)$$

where A is a thermoelectric factor (2 for zinc oxide), n is electron density, h is Plank's constant, $m_c{}^*$ is the effective mass of the electron.

After substitution of various constants Eq. (4) simplifies to [17]

$$\mathrm{Log}\, n = \frac{3}{2}\log T - 0.005\,\mathrm{TEP} + 15.719 \quad (5)$$

The electron density (n) was calculated using the above equation and was in the order of 10^{19} cm^{-3} for films annealed at 400–700 °C. The mobility (μ) of the charge carriers is determined from the relation:

$$\mu = \frac{\sigma}{ne} \quad (6)$$

where n is electron density and σ is conductivity. The variation of log n and log μ as a function of temperature for ZnO film annealed at

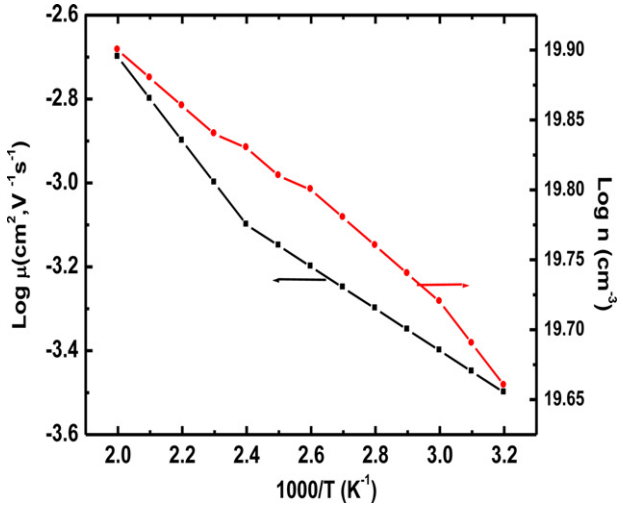

Fig. 9. Variation of log n and log μ as a function of temperature for ZnO films annealed at 700 °C.

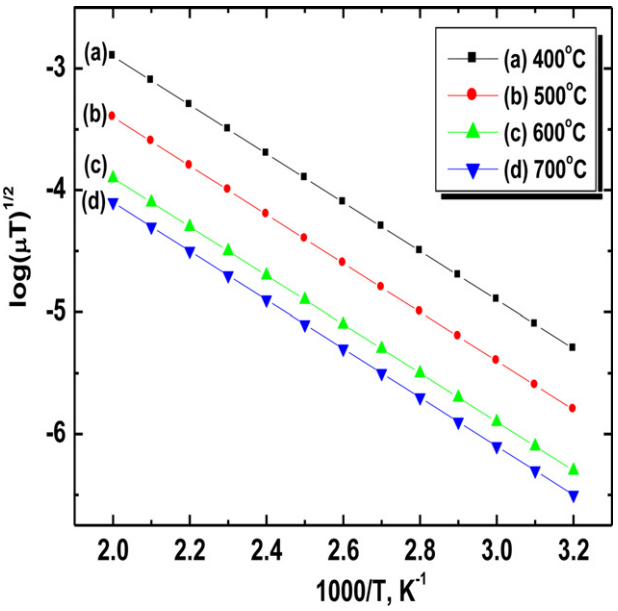

Fig. 10. Determination of intercrystalline barrier height for ZnO films annealed at 400–700 °C.

700 °C is shown in Fig. 9. It is observed that electron density (n) and mobility (μ) increases with temperature. The electron carrier concentration (n) and mobility (μ) were estimated to be of the order of 4.75–7.10 × 10^{19} cm^{-3} and 2.98–5.20 × 10^{-5} cm^2 V^{-1} S^{-1} respectively for films annealed between 400 and 700 °C. The temperature variation of carrier mobility suggests that there is a considerable amount of scattering mechanism due to the intergrain barrier potential [18–21]. This carrier scattering is temperature dependent, and therefore it is related to the carrier mobility (μ) and intergranular potential (Φ_b) [18–21].

$$\mu = \mu_o \exp\left(\frac{-\Phi_b}{kT}\right) \quad (7)$$

where all the terms have their usual meanings. Intergranular potential (scattering potential) is therefore calculated from the log $\mu T^{1/2}$ versus 1000/T variation as suggested by Micocci et al. [20]. This shown in Fig. 10 and its typical value is between 0.18 and 0.40 eV for ZnO film annealed at 400–700 °C.

3.6. Optical studies

The ZnO thin films on glass substrate were used to study the optical absorption. The optical absorption of ZnO thin films in the wavelength range of 200–1000 nm has been investigated.

Fig. 11 shows plots of $(\alpha h\nu)^2$ as a function of photon energy ($h\nu$) for ZnO thin films as a function annealing temperature (400–700 °C). Since the plots are almost linear, the direct nature of the optical transition in ZnO is confirmed. Extrapolation of these curves to photon energy axis reveals the band gaps. The optical absorption data were analyzed using the following classical relation for near edge optical absorption in semiconductor.

$$\alpha = \alpha_o \frac{(h\nu - E_g)^n}{h\nu} \quad (8)$$

where 'α_o' is a constant, 'E_g' is the semiconductor band gap and 'n' is a number equal to 1/2 for direct gap and 2 for indirect gap compound.

The band gap of ZnO film was found to be decreased from 3.32 to 3.18 eV for films annealed at 400–700 °C. The decrease in E_g with annealing temperature could be due to increase in crystalline size and reduction of defect sites. This is in good agreement with the

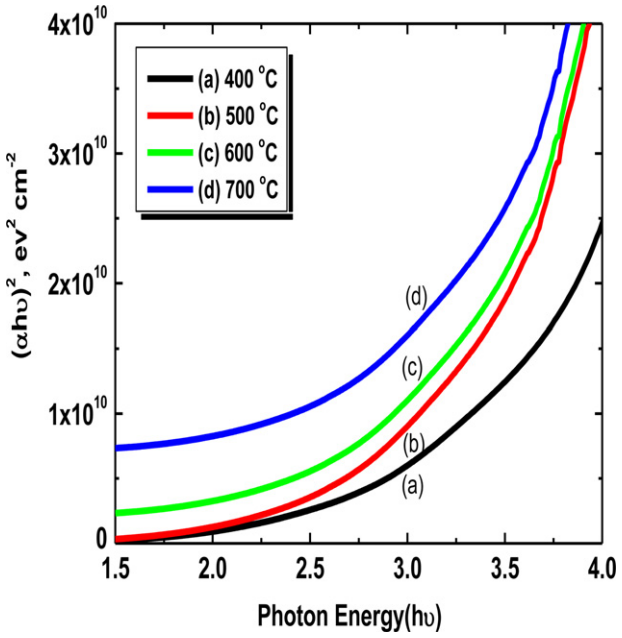

Fig. 11. Plot of $(\alpha h\upsilon)^2$ versus $(h\upsilon)$ of ZnO thin films for different annealing temperatures (400–700 °C).

experimental results of XRD analysis. According to XRD results, the mean grain size has increased with increased annealing temperature. As the grain size has increased, the grain boundary density of a film decreased, subsequently, the scattering of carriers at grain boundaries has decreased [18–22]. A continuous increase of optical constants (α and E_g) and also the shift in absorption edge to a higher wavelength with increasing annealing temperature may be attributed to increase in the particle size of the crystallites along with reduction in porosity.

The decrease in optical band gap energy is generally observed in the annealed direct-transition-type semiconductor films. Hong et al. [13] observed a shift in optical band gap of ZnO thin films from 3.31 to 3.26 eV after annealing, and attributed this shift to the increase of the ZnO grain size. Chaparro et al. [22] ascribed this 'red shift' in the energy gap, E_g, to an increase in crystallite size for the annealed ZnSe films. Bao et al. [23] also reported a decrease in E_g with increasing annealing temperature for $SrTiO_3$ thin films, and suggested that a shift of the energy gap was mainly due to both the quantum-size effect and the existence of an amorphous phase in thin films. In present case, the mean crystallite size increases from 61.82 to 73.48 nm after annealing from 400 to 700 °C. Moreover, it is understood that the amorphous phase is reduced with increasing annealing temperature, since more energy is supplied for crystallite growth, thus resulting in an improvement in crystallinity of ZnO films. Therefore, it is believed that both the increase in crystallite size and the reduction in amorphous phase cause are decreasing in band gap of annealed ZnO films. The change in optical band gap energy, E_g, reveals the impact of annealing on optical properties of the ZnO films.

4. Conclusions

Nanocrystalline zinc oxide thin films were prepared by low-cost sol gel spin coating technique. The ZnO films were annealed for various temperatures between 400 and 700 °C. The XRD results revealed that the ZnO thin film has a good nanocrystalline hexagonal wurtzite structure. The AFM analysis revealed that the surface morphology is smooth. The HRTEM analysis of ZnO thin film annealed at 700 °C confirms nanocrystalline nature of film. The SEM results depict that a uniform surface morphology and the nanoparticles are fine with an average grain size of about 40–60 nm. The dc electrical conductivity of ZnO thin films were increased from 10^{-6} to 10^{-5} $(\Omega\,cm)^{-1}$ with increase in annealing temperature. The n-type electrical conductivity is confirmed from thermo-emf measurement with no appreciable change in thermoelectric power after annealing. The electron carrier concentration (n) and mobility (μ) of ZnO films annealed at 400–700 °C were estimated to be of the order of $4.75–7.10 \times 10^{19}$ cm^{-3} and $2.98–5.20 \times 10^{-5}$ $cm^2\,V^{-1}\,S^{-1}$. Optical absorption studies show low-absorbance in IR and visible region with band gap 3.32 eV (at 400 °C) which was decreased to 3.18 eV (at 700 °C). This has been attributed to the decrease in defect levels. It is observed that ZnO thin film annealing at 700 °C after deposition provide a smooth and flat texture suited for optoelectronic applications.

Acknowledgment

Authors (VBP) are grateful to DAE-BRNS, for financial support through the scheme no. 2010/37P/45/BRNS/1442.

References

[1] B. Lin, Z. Fu, Y. Jia, Appl. Phys. Lett. 79 (2001) 943.
[2] V. Srikant, R.D. Clarke, J. Appl. Phys. 81 (1997) 6357.
[3] T. Minami, H. Nato, S. Takata, Thin Solid Films 124 (1985) 43.
[4] K.L. Chopra, S. Major, D.K. Panday, Thin Solid Films 102 (1983) 1.
[5] K.S. Weibenrieder, J. Muller, Thin Solid Films 300 (1997) 30.
[6] S. Kim, J. Yum, Y. Sung, Sol. Energy Mater. Sol. Cells 79 (2003) 495.
[7] P. Nunes, E. Fortunadeo, R. Martins, Thin Solid Films 383 (2001) 277.
[8] A.P. Roth, D.F. Williams, J. Appl. Phys. 52 (1981) 6685.
[9] Y.F. Lu, H.Q. Ni, Z.H. Mai, Z.M. Ren, J. Appl. Phys. 88 (2000) 498.
[10] X. Jiang, F.L. Wong, M.K. Fung, S.T. Lee, Appl. Phys. Lett. 83 (2003) 1875.
[11] A.E. Jimenez-Gonzalez, J.A.S. Urueta, R. Suarez-Parra, J. Cryst. Growth 192 (1998) 430.
[12] V. Gupta, A. Mansingh, J. Appl. Phys. 80 (1996) 1063.
[13] R. Hong, J. Huang, H. He, Z. Fan, Shao, Appl. Surf. Sci. 242 (3–4) (2005) 346.
[14] J.H. Lee, K.H. Ko, B.O. Park, J. Cryst. Growth 247 (1–2) (2003) 119.
[15] T.P. Gujar, V.R. Shinde, C.D. Lokhande, R.S. Mane, S.H. Han, Appl. Surf. Sci. 250 (2005) 161.
[16] V.B. Patil, S.G. Pawar, S.L. Patil, J. Mater. Sci. Mater. Electron. 21 (2010) 355.
[17] R.R. Heikes, R.W. Ure, Thermoelectricity Science and Engineering, Inter Science, 1961, p. 3.
[18] R.L. Petriz, Phys. Rev. 104 (1956) 1508.
[19] S.G. Pawar, S.L. Patil, M.A. Chougule, V.B. Patil, J. Mater. Sci. Mater. Electron. 22 (2011) 260.
[20] G. Micocci, A. Tepore, R. Rella, O.P. Sicilian, Phys. Status Solidi (a) 148 (2) (1995) 1.
[21] F.B. Michehti, P. Mark, Appl. Phys. Lett. 10 (1967) 136.
[22] A.M. Chaparro, M.A. Martinez, C. Guillen, R. Bayon, M.T. Gutierrez, J. Herrero, Thin Solid Films 361–362 (2000) 177.
[23] D. Bao, X. Yao, N. Wakiya, K. Shinozaki, N. Mizutani, Appl. Phys. Lett. 79 (2001) 3767.